Synchronized Self-Motion of Two Camphor Boats

Masahiro I. Kohira,[†,‡] Yuko Hayashima,[‡] Masaharu Nagayama,[§] and Satoshi Nakata*[,‡]

Department of Physics, Graduate School of Science, Kyoto University, CREST (Core Research for Evolutional Science and Technology) of Japan Science and Technology Corporation, Kyoto 606-8502, Department of Chemistry, Nara University of Education, Takabatake-cho, Nara 630-8528, Japan, and Research Institute for Mathematical Sciences, Kyoto University, Kyoto 606-8502, Japan

Received March 13, 2001. In Final Form: August 2, 2001

The synchronized self-motion of two camphor boats was investigated on a circular water route. Two kinds of synchronization, phase-locking and phase-oscillatory modes, could be produced by changing the temperature, the radius of the circular cell, and the mass of each boat. The nature of the synchronization is discussed in relation to the distribution of the camphor layer, which is an important factor in the driving force of self-motion. The essential features of synchronized motion were reproduced by a numerical calculation regarding the spatial distribution of the camphor layer at the air/water interface. We believe that the present results may be useful for realizing artificial motors or chemomechanical transducers, which mimic motor organs or organelles in living organisms under nonlinear and isothermal conditions.

Introduction

Autonomous motors, driven by the dissipation of chemical energy under isothermal and nonequilibrium conditions, have been studied experimentally[1] and theoretically[2−4] to create artificial chemomechanical transducers which mimic biological and molecular motors. The spontaneous motion of a liquid droplet (e.g., water, nitrobenzene, mercury, fluorocarbon, and so on) or a solid grain such as camphor has been studied extensively.[5−26] Such a spontaneous motion is generated as a result of the Marangoni effect, which is induced by a chemical or thermal gradient acting on the droplet or the grain.[5−11,22−29] The manner of such motion depends on the anisotropic distribution of the surface-active substance absorbed on the droplet[5−11] or dissolved from the solid grain.[12−21]

We previously reported the self-motion of a camphor scraping and boat at an air/water interface.[14−21] The driving force of this motion is the difference in the surface tension around the camphor scraping because the camphor molecular layer diffused from the scraping decreases the surface tension at the air/water interface. Various manners of self-motion (e.g., clockwise rotation, counterclockwise rotation, and unidirectional translation) and mode switching between rotation and translation can be produced by changing the shape of the camphor fragment.[14,15,19,20] Intermittent motion was observed for a camphoric acid scraping by changing the pH of the aqueous phase.[16−18] Recently, we reported that a camphor scraping or a camphor boat exhibits various manners of self-motion (mode switching, synchronization, mode selection) depending on the shape of the water cell.[19,20] These results suggest that a camphor scraping or camphor boat is sensitive not only to the distribution of the camphor layer but also to the boundary condition of the cell.

In this paper, phase-locking and phase-oscillatory modes of motion were produced for two camphor boats by changing the temperature of the cell, the radius of the circular cell, and the mass of each boat under the same conditions where two camphor boats were floated in the same direction on a circular water route. Such motion can be reproduced by a theoretical simulation based on a

* To whom correspondence should be addressed. Tel: +81-742-27-9191. Fax: +81-742-27-9291. E-mail: nakatas@nara-edu.ac.jp.

† Department of Physics, Kyoto University, CREST of Japan Science and Technology Corporation, and research assistance at Nara University of Education.

‡ Department of Chemistry, Nara University of Education.

§ Research Institute for Mathematical Sciences, Kyoto University.

(1) Yoshida, R.; Takahashi, T.; Yamaguchi, T.; Ichijo, H. *J. Am. Chem. Soc.* **1996**, *118*, 5134.
(2) Sekimoto, K. *Prog. Theor. Phys.* **1998**, *130*, 17.
(3) Yoshikawa, K.; Noguchi, H. *Chem. Phys. Lett.* **1999**, *303*, 10.
(4) Astumian, R. D.; Bier, M. *Phys. Rev. Lett.* **1994**, *72*, 1766.
(5) Nakata, S.; Komoto, H.; Hayashi, K.; Menzinger, M. *J. Phys. Chem. B* **2000**, *104*, 3589.
(6) Stoilov, Yu. Yu. *Langmuir* **1998**, *14*, 5685.
(7) Stoilov, Yu. Yu. *Phys.-Usp.* **2000**, *43*, 39.
(8) Bain, C.; Burnett-Hall, G.; Montgomerie, R. *Nature* **1994**, *372*, 414.
(9) Domingues dos Santos, F.; Ondarçuhu, T. *Phys. Rev. Lett.* **1995**, *75*, 2972.
(10) Brochard, F.; de Gennes, P. G. *C. R. Acad. Sci. Paris* **1995**, *321 IIb*, 285.
(11) Shanahan, M. E. R.; de Gennes, P. G. *C. R. Acad. Sci. Paris* **1997**, *324 IIb*, 261.
(12) Rayleigh, L. *Proc. R. Soc. London* **1890**, *47*, 364.
(13) Shanahan, M. *Pour la Sci.* **1998**, *244* (Feb), 106.
(14) Nakata, S.; Iguchi, Y.; Ose, S.; Kuboyama, M.; Ishii, T.; Yoshikawa, K. *Langmuir* **1997**, *13*, 4454.
(15) Nakata, S.; Hayashima, Y. *J. Chem. Soc., Faraday Trans.* **1998**, *94*, 3655.
(16) Nakata, S.; Iguchi, Y.; Ose, S.; Ishii, T. *J. Phys. Chem. B* **1998**, *102*, 7425.
(17) Nakata, S.; Hayashima, Y. *Langmuir* **1999**, *15*, 1872.
(18) Nakata, S.; Hayashima, Y.; Ishii, T. *Colloids Surf., A* **2001**, *182*, 231.
(19) Nakata, S.; Hayashima, Y.; Komoto, H. *Phys. Chem. Chem. Phys.* **2000**, *2*, 2395.
(20) Nakata, S.; Kohira, M. I.; Hayashima, Y. *Chem. Phys. Lett.* **2000**, *322*, 419.
(21) Hayashima, Y.; Nagayama, M.; Nakata, S. *J. Phys. Chem. B* **2001**, *105*, 5353.
(22) Barton, K. D.; Subramanian, R. S. *J. Colloid. Interface Sci.* **1989**, *133*, 211.
(23) Chaudhuy, M. K.; Whitsides, G. M. *Science* **1992**, *256*, 1539.
(24) de Gennes, P. G. *Rev. Mod. Phys.* **1985**, *57*, 827.
(25) de Gennes, P. G. *Physica A* **1998**, *249*, 196.
(26) Brochard, F. *Langmuir* **1989**, *5*, 432.
(27) Sackmann, E. In *Temporal Order*; Rensing, L., Jaeger, N. I., Eds.; Springer-Verlag: Berlin, 1985; pp 153−162.
(28) Scriven, L. E.; Sternling, C. V. *Nature* **1960**, *187*, 186.
(29) Landau, L. D.; Lifshits, E. M. *Fluid Mechanics*, 2nd ed.; Course of Theoretical Physics Vol. 6; Pergamon: New York, 1987.

10.1021/la010388r CCC: $20.00
Published on Web 09/28/2001

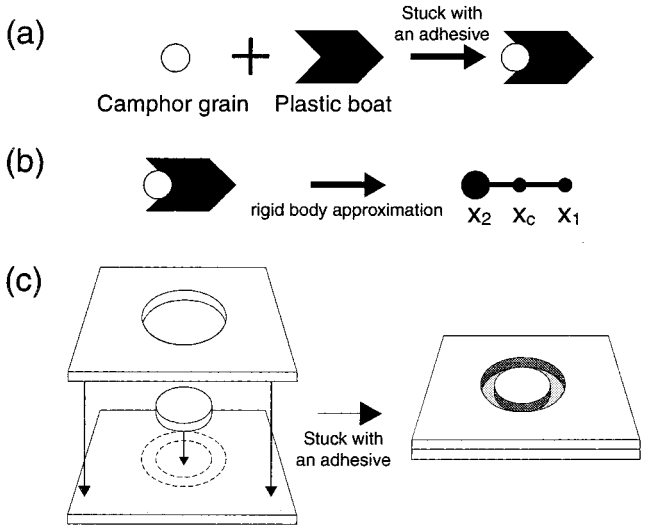

Figure 1. Schematic diagram of (a) a camphor boat (the shape of the boat was drawn using computer software and printed on a polyester sheet with a laser printer), (b) rigid body approximation for a camphor boat to make a mathematical model easily, and (c) a circular water route made of Teflon (width of the route, 5 mm; thickness, 2 mm; inner radius, 10.0, 15.0, or 20.0 mm).

Newtonian equation coupled with a reaction−diffusion equation for the camphor layer.

Experiment

(+)-Camphor was obtained from Wako Chemicals (Kyoto, Japan). Water was first distilled and then purified with a Millipore Milli-Q filtering system (pH of the obtained water, 6.3). A boat was made of polyester film (thickness, 0.1 mm) of a specific shape, and a camphor grain was stuck to its stern as schematically illustrated in Figure 1a. Two camphor boats were floated on the surface of water in a circular route made of Teflon (width of the route, 5 mm; thickness, 2 mm; inner radius, 10.0, 15.0, or 20.0 mm) in the same direction (Figure 1c). Each boat cannot overtake the other because of the narrow width of the route. The movements of the camphor boats were monitored with a digital video camera (Sony DCR-VX700) and recorded on videotape. The two-dimensional positions of the camphor boats were monitored with a minimum time resolution of 1/30 s and then analyzed by a Himawari system (Library Inc., Japan). The temperature of the water cell was changed with a thermoplate (TP-80, Iuchi Co. Ltd., Japan).

Results

Figure 2 shows snapshots of the self-motion of two camphor boats at the air/water interface (top view) at (a, b) 288 K and (c, d) 298 K. Figure 3 shows the time development of the phase difference between the two boats, $\Delta\theta$, which is defined in Figure 2. Two kinds of synchronization, phase-locking (a, b) and phase-oscillatory modes (c, d), were observed. At 288 K, phase-locking rotation between the two camphor boats (phase difference, $\Delta\theta$: (a) π, (b) $\pi/2$) was maintained for 90 s (or 60 cycles of rotation). At 298 K, phase-oscillatory rotation was maintained for 240 s in (c) and 30 s in (d). In one phase oscillation, the two boats rotated for 25 and 3 cycles in (c) and (d), respectively.

The phase difference between the two boats, $\Delta\theta$, depended on the inherent velocity of each boat without the other boat. The relationship between the phase difference, $\Delta\theta$, and the ratio of the inherent velocities of two boats, v_α/v_β, on the phase-locking mode was shown in Figure 4. In this experiment, the velocity of a single boat, which was changed depending on the mass of the boat

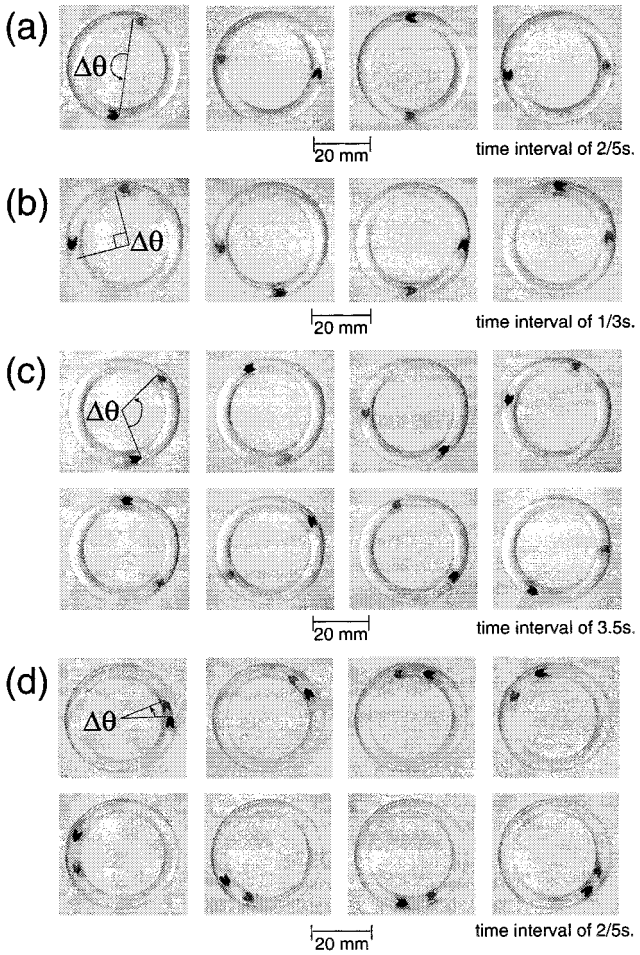

Figure 2. Snapshots of the self-motion of two camphor boats in a circular cell (top view) at (a) $t = 24.0-25.2$ s, (b) $t = 12.0-13.0$ s, (c) $t = 165.0-189.5$ s, and (d) $t = 0.0-2.8$ s after two camphor boats were floated at the air/water interface with a time interval of (a) 0.40, (b) 0.33, (c) 3.50, and (d) 0.40 s. The temperature of the water cell was (a, b) 288 K and (c, d) 298 K. The inner radius of the water route was 15.0 mm.

and the status of the attachment of a camphor grain, was 28−122 mm/s. $\Delta\theta$ approached π when v_α/v_β was increased to 1.

The stability of the phase-locking mode (constancy of $\Delta\theta$) decreased with the increase in the diameter and temperature of the circular water cell. For example, at a temperature below 288 K, the phase-locking mode was observed. At a temperature between 288 and 298 K, the phase-locking mode was stable but sometimes disrupted for several seconds (data not shown). At a temperature above 298 K, the incidence of the phase-oscillatory mode was clearly greater than that of the phase-locking mode.

Discussion

To theoretically understand the mechanism of the phase-locking and phase-oscillatory synchronization of two camphor boats, we introduce a mathematical model[13,14,21] for a camphor boat in a circular cell and solve it numerically. On the basis of the experimental results, the motion of a camphor boat in a circular cell may be considered one-dimensional motion. Therefore, we consider a one-dimensional camphor boat model with a periodic boundary condition. First, we assume that a camphor grain connected to the rear of a boat is a material particle because of its sufficiently small volume, and we

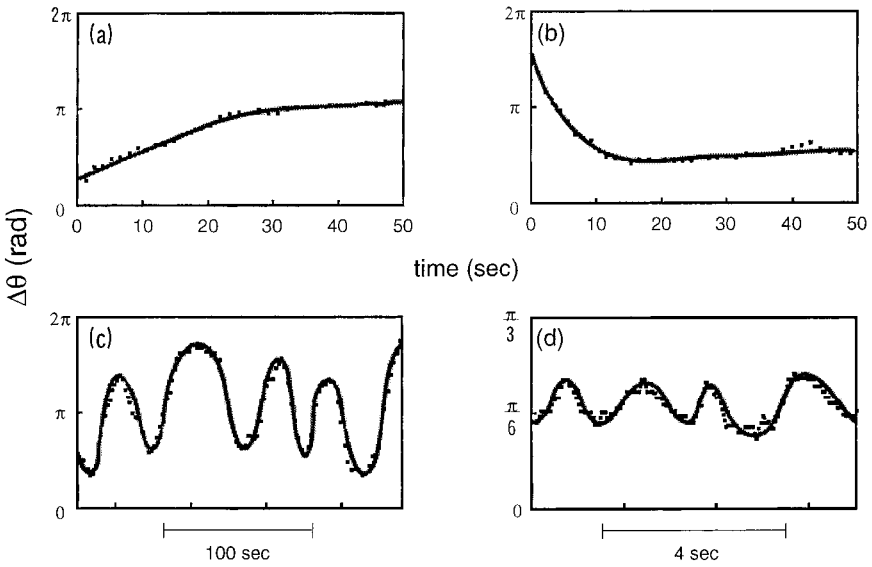

Figure 3. Time development of the phase difference between two camphor boats, $\Delta\theta$, which is defined in Figure 2. The data in (a)−(d) correspond to those in Figure 2, respectively.

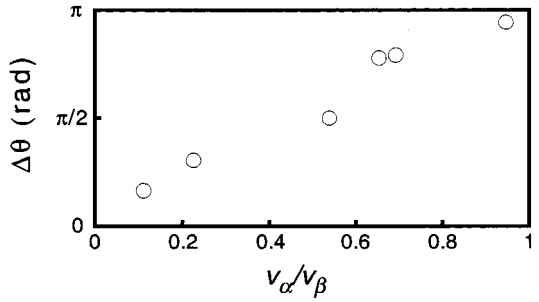

Figure 4. The relationship between the phase difference, $\Delta\theta$, and the ratio of the inherent velocities of two boats, v_α/v_β ($v_\alpha \le v_\beta$) on the phase-locking mode at 288 K. The inner radius of the water route was 15.0 mm.

also approximate a camphor boat as two rigid material particles (Figure 1b):

$$(x_1(t),x_2(t)) = (x_c(t) + l, x_c(t) - l) \quad (1)$$

where $x_1(t)$ denotes the front point of the camphor boat and x_2 is the rear point. $x_c(t)$ denotes the center of mass of the camphor boat, and $2l$ is the length of the boat. The motion of the camphor boat may then be expressed by eq 2 (see Appendix):[14,17,20,21]

$$\rho\ddot{x}_c(t) = \frac{1}{2}\sum_{j=1}^{2}\frac{\partial}{\partial x}\gamma(u(x_j(t),t)) - \mu\dot{x}_c(t) + \frac{1}{2}\sum_{j=1}^{2}e_j\frac{\partial}{\partial x}\gamma(u(x_j(t),t))\dot{x}_c(t) \quad (2)$$

where γ (N/m) is the surface tension at the air/water interface, $u(x, t)$ (mol/m^2) is the surface concentration of the camphor layer diffused from the grain, ρ (kg/m^2) is the surface density of each camphor boat, μ (N s/m^3) is the constant of the surface viscosity, and e (s/m) is the coefficient for the term for convection flow, which may be effective as a negative resistance term. The surface tension may be expressed as a function of $u(x, t)$ as follows:[19]

$$\gamma(u(x,t)) = \frac{\gamma_0}{cu(x,t) + 1} \quad (3)$$

where γ_0 (N/m) is the surface tension of water and c (m^2/mol) is constant. Next, we consider the equation for the surface concentration of the camphor layer $u(x, t)$, which is given by the reaction−diffusion equation, as follows:[19]

$$\frac{\partial u}{\partial t} = D\frac{\partial^2 u}{\partial x^2} - ku + F(u,x,x_2(t);r_0) \quad t > 0 \quad x \in \Omega \quad (4)$$

where D (m^2/s) is the diffusion coefficient of the camphor layer diffused to the air/water interface, k (1/s) is the sum of the rates of sublimation (k_1) and dissolution (k_2) of the camphor layer at the air/water interface ($k = k_1 + k_2$), r_0 is the radius of the camphor grain, and Ω is the surface area of the water bath. Now F (mol/(m^2 s)) indicates the diffusion of the camphor layer from the camphor grain to the air/water interface. Although we approximate the camphor grain to a material point in eq 2, to consider the dependence on the size of the camphor grain, we introduce the radius of the camphor grain, r_0, in F. Thus, F is expressed by eq 5:

$$F(u,x,x_2(t);r_0) = \begin{cases} h(u)S_0 & |x - x_2(t)| \le r_0 \\ 0 & |x - x_2(t)| > r_0 \end{cases} \quad (5)$$

where S_0 is the constant amount of camphor molecules to be supplied from the camphor grain, $h(u)$ is the rate of diffusion of the camphor layer from its scraping, which depends on the concentration of camphor layer, that is, $h(u) = h_0(u_0 - u)$, where u_0 is the maximum concentration of the camphor layer. We assume here that the decrease in the mass of the camphor grain by diffusion of the camphor layer is negligible, and therefore S_0, μ, and D are constant. To reproduce rotational motion in the circular cell, we assume the following periodic boundary conditions:

$$\begin{cases} u(0,t) = u(L,t) \\ \dfrac{\partial u}{\partial x}(0,t) = \dfrac{\partial u}{\partial x}(L,t) \end{cases} \quad t > 0 \quad 0 \le x < L \quad (6)$$

where L is the circumference of the circular cell ($L = 2\pi R$, R is the radius of the cell). To solve eqs 1−6, we require that $u(\cdot,t)$ is the continuously differentiable function on $(0, L)$.

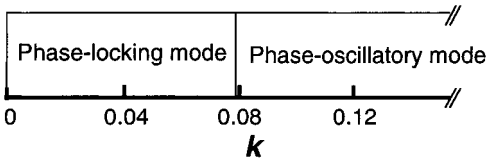

Figure 5. Phase diagram of the synchronized mode depending on k for a numerical simulation based on eqs 7−9. $\rho_i = 1.0$, $\mu_i = 0.45$, $e_i = 3.2$, $\gamma_0 = 2.0$, $c = 1.0$, $l_i = 0.2$, $D = 1.0$, $h_0 = 1.0$, $u_0 = 1.0$, $S_{i0} = 1.0$, $r_{\alpha 0} = r_{\beta 0} = 0.15$, and $L = 15.0$.

We next expand from eqs 1−6 to the following model for two camphor boats in order to investigate synchronized phenomena of the two camphor boats:

$$\begin{cases} \rho_i \ddot{x}_{ic}(t) = \dfrac{1}{2}\displaystyle\sum_{j=1}^{2} \frac{\partial}{\partial x}\gamma(u(x_{ij},t)) - \mu_i \dot{x}_{ic}(t) + \\ \qquad \dfrac{1}{2}\displaystyle\sum_{j=1}^{2} e_{ij} \frac{\partial}{\partial x}\gamma(u(x_{ij},t))\dot{x}_{ic} \qquad t > 0,\ i = \alpha,\beta \quad (7) \\ \dfrac{\partial u}{\partial t} = D\dfrac{\partial^2 u}{\partial x^2} - ku + F(u,x,x_{\alpha 2}(t);r_{\alpha 0}) + \\ \qquad F(u,x,x_{\beta 2}(t);r_{\beta 0}) \qquad t > 0,\ 0 \le x < L \quad (8) \end{cases}$$

and

$$F(x,x_{i2}(t);r_{i0}) = \begin{cases} h(u)S_{i0} & |x - x_{i2}(t)| \le r_{i0} \\ 0 & |x - x_{i2}(t)| > r_{i0} \end{cases} \quad (9)$$

where $x_{\alpha c}$ and $x_{\beta c}$ indicate the center of two camphor boats α and β, respectively.

Figure 5 shows the phase diagram of the synchronized mode depending on k for the numerical simulation based on eqs 7−9. Here, a change in k in the theoretical simulation corresponds to a change in T experimentally. In the case of small values of k, the phase-locking mode is reproduced well due to the short distance between boats and rapid distribution of the camphor layer. On the other hand, with large k, the phase-oscillatory mode is well reproduced.

Figure 6 shows the time development of the phase difference between the two camphor boats, $\Delta\theta$, for a numerical simulation based on eqs 7−9. The phase-locking (Figure 3a,b, Figure 4) and phase-oscillatory (Figure 3c,d) modes in the experiments are well reproduced theoretically by changing the radius of each grain r_{i0} and the dissipative coefficient k, as indicated in Figure 6a−d. In this simulation, $\Delta\theta$ also depends on the inherent velocities of the individual boats without another one. Figure 7 shows the profiles of the surface concentration of the camphor layer $u(x, t)$ for a numerical simulation corresponding to Figure 6a,c. In Figure 6a, the motion of a camphor boat is always affected by the camphor layer supplied by the other camphor boat, and the two boats tend to stay separated from each other at a maximal distance; that is, $\Delta\theta = \pi$. Thus, the concentration gradient of boat α, $\partial u(x_{\alpha c})/\partial x$, is maintained to be equal to that of boat β ($\partial u(x_{\alpha c})/\partial x = \partial u(x_{\beta c})/\partial x$), and therefore the phase-locking mode is generated (see Figure 6a).

On the other hand, with large k, the phase-oscillatory mode is reproduced due to rapid sublimation and dissolution of the camphor layer. At a significantly low surface concentration for the camphor layer between two camphor boats, the boats are not always sensitive to each other. When camphor boat β is placed on the rear of boat α at the initial condition ($t = 0$ in Figure 6b), the velocity of boat β decreases due to the camphor layer supplied by boat α. In the next stage, boat α remains separated from boat β because $\partial u(x_{\alpha c})/\partial x$ is larger than $\partial u(x_{\beta c})/\partial x$ ($t = 5.2$−15.6 in Figure 6b), and then boat α approaches the rear of boat β ($t = 20.8$ and 26.0 in Figure 6b). In these stages, the rates of sublimation and dissolution of the camphor layer are so large that an area with a significantly low surface concentration for the camphor layer between the two camphor boats is reproduced. Thus, the phase-oscillatory mode will be repeated while the conditions $\partial u(x_{\beta c})/\partial x > \partial u(x_{\alpha c})/\partial x$ and $\partial u(x_{\alpha c})/\partial x > \partial u(x_{\beta c})/\partial x$ alternate periodically (see Figure 7b). Figure 5 suggests that these modes can be controlled by selecting appropriate k, and

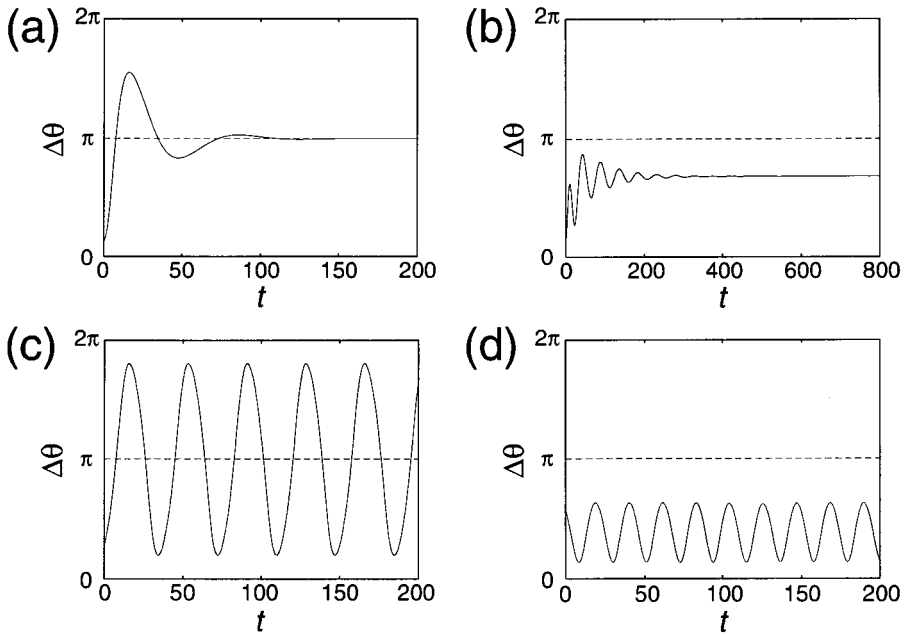

Figure 6. Time development of the phase difference between two camphor boats, $\Delta\theta$, for a numerical simulation based on eqs 7−9. $\rho_i = 1.0$, $\mu_i = 0.45$, $e_i = 3.2$, $\gamma_0 = 2.0$, $c = 1.0$, $l_i = 0.2$, $D = 1.0$, $h_0 = 1.0$, $u_0 = 1.0$, $S_{i0} = 1.0$, and $L = 15.0$. (a) $r_{\alpha 0} = r_{\beta 0} = 0.15$, $k = 0.045$; (b) $r_{\alpha 0} = 0.095$, $r_{\beta 0} = 0.195$, $k = 0.075$; (c) $r_{\alpha 0} = r_{\beta 0} = 0.15$, $k = 0.085$; (d) $r_{\alpha 0} = 0.095$, $r_{\alpha 0} = 0.195$, $k = 0.095$.

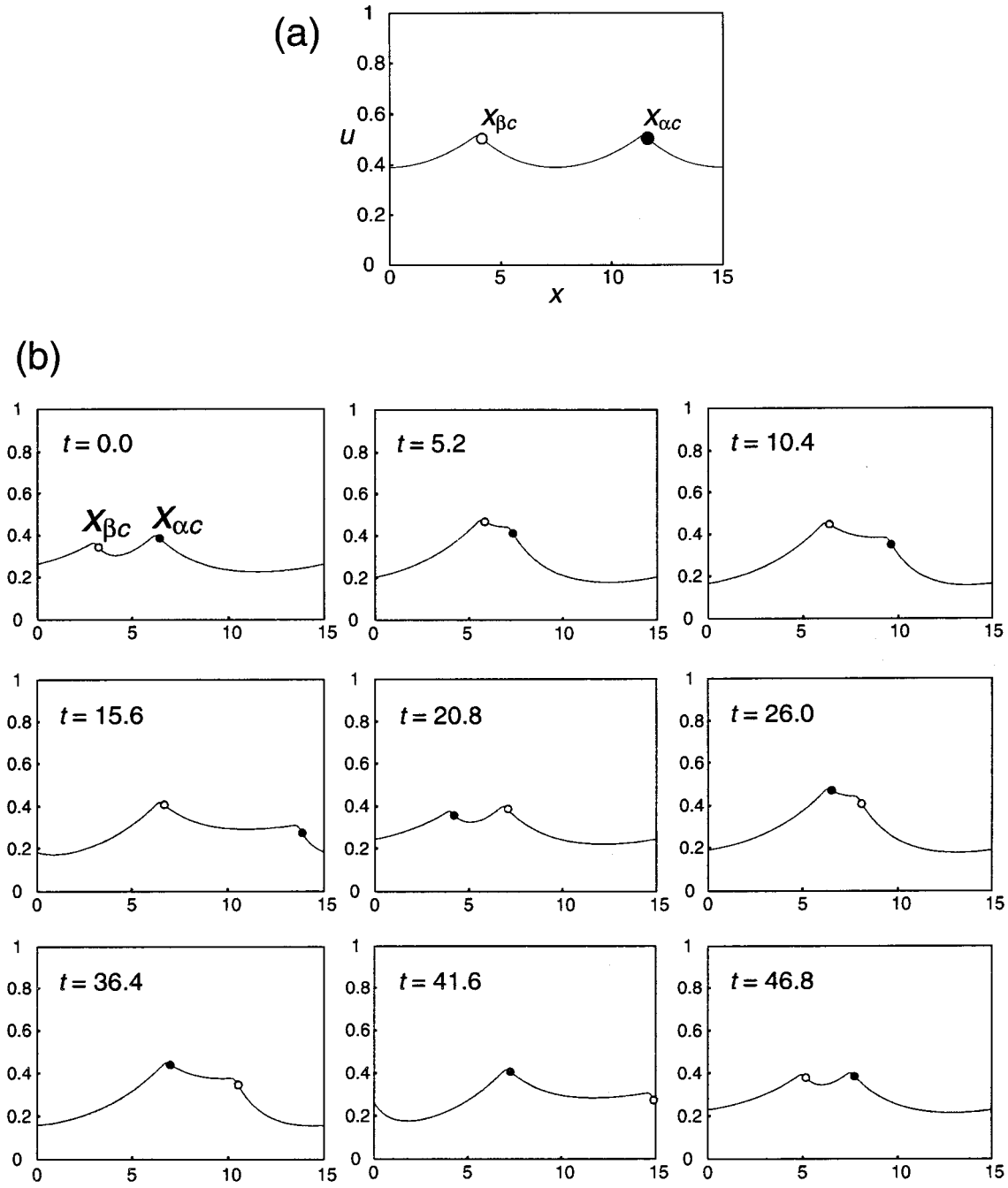

Figure 7. (a) Profile of the surface concentration of the camphor layer, $u(x, t)$, and (b) time development of the concentration of the camphor layer $u(x, t)$ with a time interval of $t = 5.2$, where (a) and (b) correspond to (a) and (c) of Figure 6. The boat α goes away from β (step I: $t = 5.2-15.6$), the boat α comes up to the boat β (step II: $t = 15.6-26.0$), the boat β goes away from the boat α (step III: $t = 26.0-41.6$), and the boat β comes up to the boat α (step IV: $t = 41.6-46.8$). Steps I−IV are repeated. Each boat cannot overtake the other numerically.

we observed this tendency statistically in the experiment. If e_i is zero in eq 7, the phase-oscillatory mode cannot be reproduced in the numerical simulation. Therefore, the convection term, which has not yet been measured experimentally, may have a suitable value to explain the dynamics of camphor boats.

As for the phase-locking mode in the experiments, the distance between two boats, $R\Delta\theta$, did not depend on v_α/v_β, but $\Delta\theta$ depended on v_α/v_β when the radius of the cell, R, was short (Figure 4). This suggests that the velocities of two camphor boats are affected by each other because of a sufficient development of the camphor layer on the small surface area of the water surface. On the other hand, $R\Delta\theta$ depended on v_α/v_β, due to the large surface area when the radius of the cell was significantly long (data not shown).

Conclusion

Two camphor boats show phase-locking and phase-oscillatory modes by changing the radius and temperature of the cell and maintain these modes while spontaneously breaking the homogeneous distribution of the camphor layer along the water route. To clarify the mechanism of these modes, a theoretical simulation based on the reaction−diffusion equation with parameters k and e_i reproduced such camphor motion, and the surface concentration of the camphor layer was then calculated using the equation. Although the hydrodynamics on the self-

motion has not been experimentally or theoretically clarified yet, the term of the convection in eq 8 plays an important role of the phase-oscillatory mode. Further studies of the hydrodynamics will theoretically provide a fuller understanding of the observed self-motion. For example, we should measure the Reynolds number in the present system to clarify the effect of the viscous resistance.[13]

According to the Curie−Prigogine theorem, a vector process cannot couple with scalar variables, such as an ideal chemical reaction, in an isotropic system under a steady state. This implies that a vectorial flow can be induced only when the reaction field is "anisotropic", such as in the present experimental system and also as seen in artificial and biological heterogeneous membranes.[30−32] We have estimated the driving force of the self-motion as the mechanochemical transducer.[15] The novel point of the present autonomous system is that a camphor boat can change both its motion and the reaction field temporally by itself depending on the shape of the field boundary. As an application of these results, the autonomous system will be able to not only create various modes depending on the outer environment but also change the reaction field including the shape of the boundary depending on the mode as a simple mode of the self-adaptation to the environment. We believe that the present study may be useful for realizing artificial motors or chemomechanical transducers, which mimic motor organs or organelles in living organisms under nonlinear and isothermal conditions.

Acknowledgment. The present study was supported in part by a Grant-in-Aid for Scientific Research from the Ministry of Education, Science and Culture of Japan, the Yamada Science Foundation, and the President Fellowship from Nara University of Education.

Appendix

We approximate the camphor boat to a two-particle rigid body and derive the Newtonian equation for each material particle as the mathematical model of the camphor boat. First, we assume that the center of the small two-dimensional rectangular domain, $(-\Delta x/2,\Delta x/2) \times (-\Delta y/2,\Delta y/2)$, is given as $(x_c(t), y_c(t))$. Then, the equation of motion for the x-component is composed of three forces, f_1, f_2, and f_3. f_1, which is generated by the difference in the surface tension between $-\Delta x/2$ and $\Delta x/2$, is expressed by eq 10:

$$f_1 = \Delta y\left(\gamma\left(u\left(x_c + \frac{\Delta x}{2}, y_c, t\right)\right) - \gamma\left(u\left(x_c - \frac{\Delta x}{2}, y_c, t\right)\right)\right) \quad (10)$$

We assume that f_2, on the surface viscosity of a material particle, is expressed by eq 11 as a simple function:

$$f_2 = -\mu\Delta x\Delta y\dot{x}_c(t) \quad (11)$$

We assume that f_3, which is generated by the convection flow, is in proportion to the difference in surface tension and is effective as negative resistance. Hence, the force of convection flow may be described by eq 12:

$$f_3 = e\Delta y\left(\gamma\left(u\left(x_c + \frac{\Delta x}{2}, y_c, t\right)\right) - \gamma\left(u\left(x_c - \frac{\Delta x}{2}, y_c, t\right)\right)\right)\dot{x}_c(t) \quad (12)$$

where e (s/m) is a coefficient of positive fixed value. As the result, we obtain the motion of x_c:

$$\rho\Delta x\Delta y\ddot{x}_c(t) = f_1 + f_2 + f_3 \quad (13)$$

where ρ is the surface density of the rectangular domain (kg/m^2). When $\Delta x \to 0$ and $\Delta y \to 0$, we have the following equation:

$$\rho\ddot{x}_c(t) = \frac{\partial}{\partial x}\gamma(u(x_c,y_c,t)) - \mu\dot{x}_c(t) + e\frac{\partial}{\partial x}\gamma(u(x_c,y_c,t))\dot{x}_c(t) \quad (14)$$

The equation of the motion for y_c is similarly obtained as eq 15:

$$\rho\ddot{y}_c(t) = \frac{\partial}{\partial y}\gamma(u(x_c,y_c,t)) - \mu\dot{y}_c(t) + e\frac{\partial}{\partial y}\gamma(u(x_c,y_c,t))\dot{y}_c(t) \quad (15)$$

In the case of one-dimensional space, the one-particle Newtonian equation becomes

$$\rho\ddot{x}_c(t) = \frac{\partial}{\partial x}\gamma(u(x_c,t)) - \mu\dot{x}_c(t) + e\frac{\partial}{\partial x}\gamma(u(x_c,t))\dot{x}_c(t) \quad (16)$$

Therefore, the Newtonian equations for two particles $x_1(t)$ and $x_2(t)$ are

$$\rho\ddot{x}_1(t) = \frac{\partial}{\partial x}\gamma(u(x_1,t)) - \mu\dot{x}_1(t) + e\frac{\partial}{\partial x}\gamma(u(x_1,t))\dot{x}_1(t) \quad (17)$$

and

$$\rho\ddot{x}_2(t) = \frac{\partial}{\partial x}\gamma(u(x_2,t)) - \mu\dot{x}_2(t) + e\frac{\partial}{\partial x}\gamma(u(x_2,t))\dot{x}_2(t) \quad (18)$$

respectively. From eq 1, which is a restraint condition, we obtain the relation $\dot{x}_1 = \dot{x}_2 = \dot{x}_c$ and $\ddot{x}_1 = \ddot{x}_2 = \ddot{x}_c$. Consequently, eq 2 is obtained by eqs 17 and 18.

LA010388R

(30) Katchalsky, A.; Curie, P. F. *Nonequilibrium Thermodynamics in Biophysics*; Harvard University Press: Cambridge, 1965.
(31) Prigogine, I. *Introduction to the Thermodynamics of Irreversible Processes*, 2nd ed.; John Wiley & Sons: New York, 1961.
(32) Bocca, N. *Symmetries and Broken Symmetries in Condensed Matter Physics*; IDSET: Paris, 1981.